CHARACTERIZATION OF VIBRATION-INDUCED IMAGE DEFECTS IN INPUT SCANNERS

Robert P. Loce
Xerox Corporation
Corporate Research and Technology
Webster, NY 14580
loce.wbst147@xerox.com

George Wolberg
Department of Computer Science
City College of New York / CUNY
New York, NY 10031
wolberg@cs-mail.engr.ccny.cuny.edu

ABSTRACT

Typical office scanners employ a moving linear-sensor array or moving optics. the velocity of the components is generally not constant in time. It may be modulated directly (at one or more frequencies) by dynamic errors of gears, timing bets, and motors, and indirectly by structural vibrations induced by gears, fans, etc. Nonuniform velocity is known to cause undesirable brightness fluctuation and warping in the sampled image. The present paper characterizes the image defects induced by nonuniform velocity. A companion paper utilizes the degradation information to develop an algorithm to restore the degraded image.

Keywords: image defects, digital documents, scanned documents, vibrations, motion quality

1. INTRODUCTION

In a document scanner, a linear sensor array (LSA) passes over a document, ideally, at uniform velocity. The output of a single photosensor in the LSA is proportional to the integrated irradiance received by the sensor as it scans through an exposure region. When vibratory motion of the sensor array is considered, the actual size of the exposure region is time-varying. This introduces artifacts such as brightness fluctuation and geometric warping. In this paper, we characterize these image defects.

The effect of motion on the resolution of *analog* imaging systems has been studied extensively. The problem typically addressed concerns characterization of the image blur caused by motion during the integration time of a photosensitive imaging medium. In this typical case the blur is usually constant throught the image and may be caused by linear or vibratory motion. The blur is constant because the devices under study acquire the full spatial extent of the image at one time, as in a conventional photographic camera. Characterization of this spatial uniform blur leads to a deconvolution-type image restoration algorithm. The present paper differs from that body of work in that we are concerned with images that are digitized in a scan line fashion where each scan line may be acquired with a different arbitrary velocity of the light sensing array. For more information on the uniform blur case see [1, 2, 3].

Several authors have considered the effects of nonuniform photoreceptor motion and other sources of noise in slit scanning photocopiers and digital printers. Loce and Lama [4] characterized the periodic exposure level error caused by vibration in a slit scanning photocopier. Bestenreiner, Geis, Helmberger, and Stadler [5], Takiguchi, Miyagi, Okamura, Ishoshi, and Shibata [6], and Haas [7] examined the effects of periodic scan line position errors when printing periodic binary patterns (e.g., halftones). Schubert [8] and Firth, Kessler, Muka, Noar and Owens [9] analyzed banding in continuous tone prints due to periodic errors. Burns, Rabbani and Ray [10], and Melnychuck and Shaw [11] concentrated on the effect of random errors in the continuous tone and binary cases, respectively. Bloomberg and Engeldrum [12] analyzed the color error on a print that is caused by random pixel placement errors. Loce and Lama [13] employed exposure and xerographic models to examine vibration induced halftone banding in image bar printers. Loce, Lama and Maltz [14] examined the effects of raster position error in a xerographic laser printer and focused on the parametric dependences of halftone banding in the resulting prints.

This paper describes the basic operation of a moving photosensor and the problem of vibrations in input scanners. An analysis and examples of image defects for several special cases is given. A companion paper [16] utilizes the degradation information to develop an algorithm that restores the degraded image.

2. THE PROBLEM OF VIBRATION IN INPUT SCANNERS

In this section we review the basic problem of input scanning. First, we consider sampling in the time domain. Then we cast the problem into the spatial domain for uniform and nonuniform velocities.

2.1 Sampling in the Time Domain

Consider the output of a single photosensor in an LSA. Let $H(x)$ be the image irradiance distribution, and let $S(x - X(t))$ be the static photosensor sensitivity profile positioned at $X(t)$ at time t (see Fig. 1).

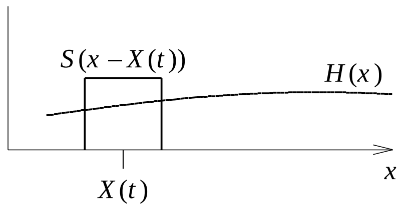

Figure 1: Photosensor sensitivity and image irradiance.

The instantaneous charge $C(X(t))$ generated by the photosensor is given by the product of the irradiance distribution and photosensor sensitivity profile integrated over space:

$$C(X(t)) = \int_{-\infty}^{\infty} H(x)\, S(x - X(t))\, dx \ . \tag{2.1}$$

This cross-correlation integral can be written as a convolution:

$$C(X(t)) = H(X(t)) * S(-X(t)) \ . \tag{2.2}$$

Digitization is performed by integrating, or accumulating, the instantaneous charge for a period of time T_{acc}, and then sampling it at temporal intervals T_s, where $T_{acc} \le T_s$. The nth sample is given by

$$F(n) = \int_{nT_s}^{nT_s + T_{acc}} C(X(t))\, dt = \int_{nT_s}^{nT_s + T_{acc}} H(X(t)) * S(-X(t))\, dt \ . \tag{2.3}$$

The integration in Eq. (2.3) can be replaced by convolution with a *rect* function to yield

$$\begin{aligned} F(t) &= \sum_n \delta(t - nT_s) \left[rect\left[\frac{t}{T_{acc}} \right] * C(X(t)) \right] \\ &= \sum_n \delta(t - nT_s) \left[H(X(t)) * K(t) \right] \ , \end{aligned} \tag{2.4}$$

where $K(t) = rect(t / T_{acc}) * S(-X(t))$ and

$$rect(t) = \begin{cases} 1 & -0.5 < t \le 0.5 \\ 0 & \text{otherwise} \end{cases} \ . \tag{2.5}$$

Note that the constant offset in *rect*, i.e., $T_{acc}/2$, has been omitted for notational convenience. Also, note that the array of Dirac delta δ functions allows us to write the collection of samples as a temporal function by sampling the accumulated charge with period T_s.

The accumulated charge is seen to be the convolution of the image irradiance distribution H with a kernel K that combines the effects of sensitivity function S and the motion blur incurred during the accumulation time T_{acc}. While S may be referred to as the *static integration aperture*, we refer to K as the *dynamic integration aperture* because it takes motion blur into account. If we assume that S is rectangular in form and the LSA is moving at uniform velocity during the accumulation time, then K takes a trapezoidal form. Nonuniform velocity gives rise to distortions of the trapezoid.

The sampling electronics digitize an image irradiance distribution over equal intervals in time. It is therefore straightforward to write the collection of samples as a temporal function, as seen above. However, we are interested in the effect of vibratory motion on the digitized image. For the purpose of analyzing image defects, the influence of vibration is best understood by recasting F in terms of spatial coordinate x. The next two sections apply a change of coordinates to the expressions given above to demonstrate the cases of uniform and nonuniform photosensor motion.

2.2 Sampling in the Spatial Domain: Uniform Velocity

Consider the case where the LSA velocity is constant with value V_0. The position function $X(t)$ is

$$X(t) \;=\; V_0 t \;, \tag{2.6}$$

and the instantaneous charge may be written as

$$C(X(t)) \;=\; H(X(t)) * S(-X(t)) = H(V_0 t) * S(-V_0 t)\,. \tag{2.7}$$

Performing the change of variables

$$dX = V_0\,dt \;,\quad X_s = V_0\,T_s \;,\quad X_{acc} = V_0\,T_{acc} \;, \tag{2.8}$$

the collection of samples in Eq. (2.3) now becomes

$$F(n) \;=\; \int_{nT_s}^{nT_s+T_{acc}} H(V_0 t) * S(-V_0 t)\,dt \;=\; V_0^{\;-1} \int_{nX_s}^{nX_s+X_{acc}} H(X(t)) * S(-X(t))\,dX \;. \tag{2.9}$$

Analogous to the temporal representation, the integration above can be replaced by convolution with a *rect* function to yield

$$\begin{aligned} F(X) \;&=\; V_0^{\;-1} \left(rect\!\left(\frac{X}{X_{acc}} \right) * C(X) \right) \sum_n \delta(X - nX_s) \\ &=\; V_0^{\;-1} \left(H(X) * K(X) \right) \sum_n \delta(X - nX_s)\,, \end{aligned} \tag{2.10}$$

where $K(X) = rect(X/X_{acc}) * S(-X)$. Again, an idealized rectangular approximation of S results in a trapezoidal form for K.

2.3 Sampling in the Spatial Domain: Nonuniform Velocity

LSA velocity nonuniformity tends to be vibratory (periodic). Consequently, it is convenient to express the velocity $V(t)$ as a Fourier series:

$$V(t) \;=\; V_0 + \sum_i A_i \sin(2\pi f_i t + \phi_i)\,, \tag{2.11}$$

where A_i, f_i, and ϕ_i are the velocity error amplitude, temporal frequency, and phase, respectively, for the ith frequency component. The LSA position $X(t)$ is determined from the instantaneous velocity $V(t)$:

$$X(t) \;=\; \int_0^t V(t')\,dt' \;=\; V_0 t + \sum_i \frac{A_i}{2\pi f_i} \left(\cos(\phi_i) - \cos(2\pi f_i t + \phi_i) \right) \;. \tag{2.12}$$

Note that the following inequality holds in practice and is useful for further analysis and approximation:

$$V_0 >> \sum_i A_i \ . \tag{2.13}$$

The velocity error amplitudes are typically less than 1% of the nominal velocity V_0.

We can express $F_{vib}(n)$, the samples taken in the presence of vibrations, by substituting $X(t)$ into Eq. (2.3). To recast the integral in spatial coordinates, we change the limits of integration and derive an expression for dt/dX:

$$F_{vib}(n) = \int_{nT_s}^{nT_s+T_{acc}} C(X(t))\, dt = \int_{V_0 nT_s+\xi_{n,0}}^{V_0(nT_s+T_{acc})+\xi_{n,1}} C(X(t)) \frac{dt}{dX} dX \ , \tag{2.14}$$

where $\xi_{n,0}$ and $\xi_{n,1}$ are the spatial deviations of the LSA from the nominal positions at times nT_s and $nT_s + T_{acc}$, respectively. The limits of integration mark both ends of the span over which the photosensor integration process takes place. The position errors $\xi_{n,0}$ and $\xi_{n,1}$ are defined as

$$\xi_{n,0} = \sum_i \frac{A_i}{2\pi f_i} \left[\cos(\phi_i) - \cos(2\pi f_i nT_s + \phi_i) \right] \ ,$$

$$\xi_{n,1} = \sum_i \frac{A_i}{2\pi f_i} \left[\cos(\phi_i) - \cos(2\pi f_i nT_s + T_{acc} + \phi_i) \right] \ . \tag{2.15}$$

The term dt/dX serves to weigh the instantaneous charge with the time exposure for all positions across the accumulation interval. We derive an approximation for dt/dX by taking a first-order truncated Taylor series approximation to the reciprocal of the velocity,

$$\frac{dt}{dX} = V(t)^{-1} \approx V_0^{-1} - V_0^{-2} \sum_i A_i \sin(2\pi f_i t + \phi_i) \ , \tag{2.16}$$

and substituting the first-order dependence for t, i.e., $t = X/V_0$, in Eq. (2.16). This yields a result that is expressed independently of t:

$$\frac{dt}{dX} = V(t)^{-1} \approx V_0^{-1} - V_0^{-2} \sum_i A_i \sin(2\pi f_i X / V_0 + \phi_i) \ . \tag{2.17}$$

We thus have

$$F_{vib}(n) = \int_{nX_s+\xi_{n,0}}^{nX_s+X_{acc}+\xi_{n,1}} C(X) \left[V_0^{-1} - V_0^{-2} \sum_i A_i \sin(2\pi\beta_i X + \phi_i) \right] dX \ , \tag{2.18}$$

where $X_s = V_0 T_s$ is the nominal spatial sampling period and $\beta_i = f_i / V_0$ is the ith spatial frequency of the vibration.

From Eq. (2.18) we see that the nonuniform velocity affects the charge accumulation integral in two ways: the integration limits are changed and a second term appears that is a low amplitude sum of sinusoids. These two respective effects may be thought of as FM and AM modulation of the image signal by the vibration. They are tightly coupled because the sum of sinusoids serves to compensate for the changing integration limits, which vary only because we are integrating in space rather than time. The role of these effects can best be appreciated by considering their influence in maintaining a flat-field response when imaging a region of constant intensity in the presence of vibrations.

We are interested in considering vibration frequencies corresponding to spatial frequencies at which the eye is most sensitive. Because the spatial periods of interest ($1/\beta_i \approx 1$ mm) tend to be long compared to the sampling integration distance ($X_{acc} \approx 0.057$ mm), each sine function may be approximated by its value at the center of the range of integration. This amounts to using a piecewise constant model for the sinusoids. Let

$$\xi_{n,ctr} = \frac{X_{acc} + \xi_{n,1} - \xi_{n,0}}{2} \ . \tag{2.19}$$

The set of samples becomes

$$F_{vib}(n) = \left(V_0^{-1} - V_0^{-2} \sum_i A_i \sin(2\pi\beta_i (nX_s + \xi_{n,ctr}) + \phi_i) \right) \int_{nX_s + \xi_{n,0}}^{nX_s + X_{acc} + \xi_{n,1}} C(X)\, dX \;. \tag{2.20}$$

Representing this result in spatial form yields an expression similar to Eq. (2.10):

$$\begin{aligned} F_{vib}(X) &= \sum_n W_n \left(rect\left(\frac{X}{2\xi_{n,ctr}} \right) * C(X) \right) \delta(X - nX_s) \\ &= \sum_n W_n \left(H(X) * K_{vib}(X) \right) \delta(X - nX_s) \;, \end{aligned} \tag{2.21}$$

where

$$K_{vib}(X) \;=\; S(X) * rect\left(\frac{X}{2\xi_{n,ctr}} \right) \;, \tag{2.22}$$

$$W_n \;=\; V_0^{-1} - V_0^{-2} \sum_i A_i \sin(2\pi\beta_i (nX_s + \xi_{n,ctr}) + \phi_i) \;. \tag{2.23}$$

As in the uniform velocity case, an idealized rectangular approximation of S results in a trapezoidal form for K. However, in the present nonuniform velocity case, the dimensions and offset of the trapezoid varies for each sample point. Note that W_n scales the trapezoid such that its height is inversely proportional to its width. A good approximation to W_n is the linear expression $1/(X_{acc} + \xi_{n,1} - \xi_{n,0})$.

3. ANALYSIS OF IMAGE DEFECTS FOR SPECIAL CASES

In this section, we examine the image artifacts induced by vibrations for several specific image types. The artifacts are examined by deriving the image irradiance viewed by the sensor as a function of time.

3.1 Uniform Input Image

Consider the area sample expression of Eq. (2.3). Because H is constant for a uniform image, the integrand becomes a constant C, and the integral of Eq. (2.3) becomes the constant CT_{acc}. Vibrations do not affect samples taken of a uniform image.

3.2 Linear Input Image

Consider an image with a simple linear ramp spatial irradiance distribution:

$$H(x) \;=\; hx \,, \quad x > 0 \;. \tag{3.1}$$

Assume the LSA position function is given by a sum of sinusoids:

$$X(t) \;=\; V_0 t + \sum_i A_i \sin(2\pi f_i t + \phi_i) \;. \tag{3.2}$$

The irradiance observed by the LSA over time may be obtained by substituting the position function into the irradiance distribution,

$$H(X(t)) \;=\; h\, V_0 t + h \sum_i A_i \sin(2\pi f_i t + \phi_i) \;. \tag{3.3}$$

We see that the vibration introduces frequency components into the irradiance distribution that are equivalent to the vibration frequencies. The amplitudes are scaled by the slope of the input irradiance distribution.

3.3 Sinusoidal Input Image

Consider a sinusoidal input image with spatial frequency ν and phase zero. The irradiance may be written

$$H(x) = H_0 + h \sin(2\pi\nu x) . \tag{3.4}$$

To simplify the analysis, assume a single temporal frequency of vibration f with zero phase,

$$X(t) = V_0 t + A \sin(2\pi f t) . \tag{3.5}$$

The irradiance observed by the LSA over time may be written by substituting the position expression into the formula for the irradiance distribution,

$$H(X(t)) = H_0 + h \sin[2\pi\nu(V_0 t + A \sin(2\pi f t))] . \tag{3.6}$$

To decompose the irradiance into frequency components, first employ

$$\sin(x + y) = \sin(x)\cos(y) + \cos(x)\sin(y) . \tag{3.7}$$

The irradiance becomes

$$\begin{aligned} H(X(t)) = {} & H_0 + h \sin[2\pi\nu V_0 t] \cos[2\pi\nu A \sin(2\pi f t))] \\ & + h \cos[2\pi\nu V_0 t] \sin[2\pi\nu A \sin(2\pi f t))] . \end{aligned} \tag{3.8}$$

Next, employ the Bessel expansion for sinusoids with sinusoidal arguments [15]:

$$\cos(z \sin(\theta)) = J_0(z) + 2\sum_{k=1}^{\infty} J_{2k}(z)\cos(2k\theta) , \tag{3.9a}$$

$$\sin(z \sin(\theta)) = 2\sum_{k=1}^{\infty} J_{2k+1}(z)\sin((2k+1)\theta) . \tag{3.9b}$$

The irradiance may be written

$$\begin{aligned} H(X(t)) = {} & H_0 \\ & + h \sin[2\pi\nu V_0 t] \left[J_0(2\pi\nu A) + 2\sum_{k=1}^{\infty} J_{2k}(2\pi\nu A)\cos[(2k)(2\pi f t)] \right] \\ & + h \cos[2\pi\nu V_0 t] \left[2\sum_{k=0}^{\infty} J_{2k+1}(2\pi\nu A)\sin[(2k+1)(2\pi f t)] \right] \end{aligned}$$

$$\begin{aligned} = {} & H_0 + h \sin[2\pi\nu V_0 t]\, J_0(2\pi\nu A) \\ & + 2h\sum_{k=1}^{\infty} J_{2k}(2\pi\nu A)\cos[(2k)(2\pi f t)] \sin[2\pi\nu V_0 t] \\ & + 2h\sum_{k=0}^{\infty} J_{2k+1}(2\pi\nu A)\sin[(2k+1)(2\pi f t)] \cos[2\pi\nu V_0 t] . \end{aligned} \tag{3.10}$$

To arrive at an expression with additive sinusoidal components, employ

$$\cos(x)\sin(y) = \frac{\sin(x + y) - \sin(x - y)}{2} . \tag{3.11}$$

The irradiance may be written as

$$
\begin{aligned}
H(X(t)) \;=\; & H_0 + h\sin[2\pi\nu V_0 t]\, J_0(2\pi\nu A) \\
& + h\sum_{k=1}^{\infty} J_{2k}(2\pi\nu A)\left[\sin[(2k)(2\pi f t)) + (2\pi\nu V_0 t)] - \sin[(2k)(2\pi f t) - (2\pi\nu V_0 t)]\right] \\
& + h\sum_{k=0}^{\infty} J_{2k+1}(2\pi\nu A)\left[\sin[(2k+1)(2\pi f t)) + (2\pi\nu V_0 t)] + \sin[(2k+1)(2\pi f t) - (2\pi\nu V_0 t)]\right]
\end{aligned}
$$

$$
\begin{aligned}
=\; & H_0 + h\sin[2\pi\nu V_0 t]\, J_0(2\pi\nu A) \\
& + h\sum_{k=1}^{\infty} J_{2k}(2\pi\nu A)\left[\sin[(2\pi t)(2kf + \nu V_0)] - \sin[(2\pi t)(2kf - \nu V_0)]\right] \\
& + h\sum_{k=0}^{\infty} J_{2k+1}(2\pi\nu A)\left[\sin[(2\pi t)(2k+1)f + \nu V_0)] + \sin[(2\pi t)((2k+1)f - \nu V_0)]\right] \;. \qquad (3.12)
\end{aligned}
$$

We see that the irradiance distribution is given by the input sinusoidal distribution, scaled by a constant, plus a scaled component at the vibration frequency, plus a series of ‘‘beats’’ between multiples of the vibration frequency and the input image frequency. To more clearly see the beat effect, we examine the lowest order terms. Using only the lowest order terms of each series, H becomes

$$
\begin{aligned}
H(X(t)) \;=\; & H_0 + h\sin[2\pi\nu V_0 t]\, J_0(2\pi\nu A) \\
& + hJ_1(2\pi\nu A)\left[\sin[(2\pi t)(f + \nu V_0)] - \sin[(2\pi t)(f - \nu V_0)]\right] \\
& + hJ_2(2\pi\nu A)\left[\sin[(2\pi t)(2f + \nu V_0)] - \sin[(2\pi t)(2f - \nu V_0)]\right] \;. \qquad (3.13)
\end{aligned}
$$

The lowest order beats occur at the sum and difference of the image frequency and vibration frequency, while the second order beats occur at the sum and difference of the image frequency with two times the vibration frequency. Note that the vibration frequency itself is not present in the scanned image.

4. EXAMPLES

Consider the periodic line image of Fig. 2a, with a spatial period of 1.48 cycles/mm that digitizes to four black and four white pixels at 300 spi. In Fig. 2b, we applied the scanner simulation equations with a single frequency of vibration at 1 cycle/mm with a velocity amplitude error of 20%. The lowest beat frequency occurs at 0.48 cycle/mm and is the most noticeable image defect. Note that extremely large errors were used here to render the defects in an obvious form. Additional examples are shown in [16].

5. SUMMARY

We have reviewed the basic digitization operations of an image input scanner. It has been shown how vibratory motion of the sensor area can lead to image defects such as brightness fluctuation and warping. A companion paper utilizes the above degradation analysis to develop an image processing algorithm to produce a digital image that appears to have been scanned with uniform motion.

6. ACKNOWLEDGEMENTS

This work was supported in part by NSF PYI award IRI-9157260, PSC-CUNY grant RF-665313, and a grant from the Xerox Foundation.

7. REFERENCES

(a) (b)

Figure 2: (a) Periodic line image; (b) distorted image.

[1] S. C. Som, ''Analysis of the effect of linear smear on photographic images,'' *J. Opt. Soc. Am.* 61, 859-864 (July 1971).

[2] D. Wulich and N. S. Kopeika, ''Image resolution limits resulting from mechanical vibrations,'' *Opt. Eng.* 26(6), 529-533 (June 1987).

[3] O. Hader, I. Dror, and N. S. Kopeika, ''Image resolution limits resulting from mechanical vibrations. Part IV: real-time numerical calculation of optical transfer functions and experimental verification,'' *Opt. Eng.* 33(2), 566-577 (Feb 1994).

[4] R. Loce and W. Lama, ''Exposure Strobing in Photocopiers,'' *Journal of Imaging Science*, 32(6), 238-247 (Nov/Dec 1988).

[5] F. Bestenreiner, U. Geis, J. Helmberger, and K. Stadler, ''Visibility and Correction of Periodic Interference Structures in Line-by-Line Recorded Images,'' *J. Appl. Phot. Engr.* 2, 86-92 (1976).

[6] K. Takiguchi, T. Miyagi, A. Okamura, H. Ishoshi, and F. Shibata, ''Effect of Photoreceptor Drum Rotational Speed Variation on Laser Beam Printer Halftone Reproduction,'' *Proceedings of the SPSE Third International Congress: Recent Advances in Non–Impact Printing Technologies*, 168-172, San Francisco (8/86).

[7] D. Haas, ''Contrast Modulation in Halftone Images Produced by Variation in Scan Line Spacing,'' *J. Imaging Tech.* 15, 46 (1989).

[8] P. Schubert, ''Periodic Image Artifacts from Continuous-Tone Laser Scanners,'' *Appl. Opt.* 25(21) 3880-3884 (1986).

[9] R. Firth, D. Kessler, E. Muka, M. Noar, and J. Owens, ''A Continuous Tone Laser Color Printer,'' *J. Imaging Tech.* 14, 78 (1988).

[10] P. Burns, M. Rabbani, and L. Ray, ''Analysis of Image Noise due to Position Errors in Laser Writers,'' *Appl. Opt.* 25, 2158-2168 (1986).

[11] P. Melnychuck and R. Shaw, ''Fourier Spectra of Digital Halftone Images Containing Dot Position Errors,'' *J. Opt. Soc. Am.* 5(8), 1328-1338 (1988).

[12] S. Bloomberg and P. Engeldrum, ''Color Error due to Pixel Placement Errors in a Dot Matrix Printer,'' *Proceedings of the SPSE Third International Congress: Recent Advances in Non-Impact Printing Technologies*, 257-260 (Aug 1986).

[13] R. Loce and W. Lama, ‘‘Halftone Banding due to Vibrations in a Xerographic Image Bar Printer,’’ *Journal of Imaging Technology*, 16(1), 6-11 (1990).

[14] R. Loce, W. Lama, and M. Maltz, ‘‘Modeling Vibration-Induced Halftone Banding in a Xerographic Laser Printer,’’ to appear in *Journal of Electronic Imaging*.

[15] M. Abramowitz and I. A. Stegun, *Handbook of Mathematical Functions*, National Bureau of Standards, 1964.

[16] G. Wolberg and R. Loce, ‘‘Restoration of Images Degraded by Input Scanner Vibrations,’’ *IS&T/SPIE Symposium on Electronic Imaging Science & Technology*: *Document Processing II* (these proceedings), Feb. 1995.